TIME AND SPACE SCALES OF WATER MOVEMENTS AT A MID-CENTRAL BASIN SITE

by
F. M. Boyce, F. Chiocchio

revised July 1986
NWRI Contribution # 86-22

ABSTRACT/EXECUTIVE SUMMARY

Current meter and thermistor string records made at a mid-basin site from May, 1979 through February 1980, and during August, 1980 are used to determine the time and space scales of horizontal motion in mid lake and to relate these to the major forcing variables. Motions at frequencies larger than 0.125 cycles per hour are horizontally coherent over a few km only, whereas lower frequency motions may cohere significantly over tens of km in the stratified season. Highest current speeds are associated with circularly polarized clockwise rotating motion at the inertial period at 15 m depth above the main thermocline. Surveillance cruise data shows the mid Central Basin array to be located in a zone of relatively flat thermocline topography but suggests that internal pressure gradients might at times be large enough to influence bottom flow. Limited small-scale sampling in the vicinity of the mid-basin array shows the existence of intense but small scale (5 km) internal pressure gradients that are undersampled by the array of thermistor strings (separated by 10 km). A simple diagnostic model of locally driven (pressure gradients and wind stress) currents appropriate to a region of constant depth is proposed. This model and multivariate statistical techniques in the frequency domain are used to show that the internal pressure gradients as measured by the array of thermistor strings are of marginal dynamic significance

(although the smaller scale gradients may contribute substantially to the observed variance) and to suggest that the locally driven model (wind stress near the surface and pressure gradients from wind set-up near the bottom) accounts for some of the observed relation between winds and currents. Evidence for the two-gyre mode of wind driven circulation in closed basins is also found. Many of the observed features of circulation, including seasonal evolution, can be related to the role of stratification in governing the vertical distribution of turbulent mixing.

SOMMAIRE ET RÉSUMÉ ADMINISTRATIF

Les relevés effectués au moyen de moulinets et de chaînes à thermistances au milieu d'étendues d'eau de mai 1979 à février 1980 et en août 1980 ont servi à établir les échelles de mesure du temps et de l'espace permettant de décrire les mouvements horizontaux qui animent l'eau au centre des lacs et de les appliquer aux variables caractérisant les principales forces agissantes. Les mouvements à des fréquences dépassant 0,125 cycle par heure conservent leur cohérence horizontale sur quelques kilomètres seulement tandis que les mouvements de fréquences plus basses peuvent demeurer cohérents de façon marquée sur des distances de plusieurs dizaines de kilomètres pendant la période de stratification thermique. Les courants les plus rapides engendrent des mouvements giratoires polarisés de période inertielle, tournant dans le sens des aiguilles d'une montre, à une profondeur de 15m au-dessus de la thermocline principale. Les données recueillies par les navires de recherche hydrologique ont révélé que le réseau d'instruments déployés au centre du bassin se situe dans une zone où la topographie de la thermocline est relativement uniforme. Il semble toutefois que les gradients de pression interne puissent par moment atteindre des niveaux suffisants pour agir sur les courants en profondeur. Un échantillonnage à petite échelle d'une zone limitée dans les parages du réseau au centre du bassin a mis en évidence la présence de gradients de pression interne abrupts qui, en raison de leur faible étendue (5 km), sont sous-échantillonnés par les chaînes à thermistances (déployées tous les 10 km). On propose un modèle simple qui permettrait de diagnostiquer, pour une région de profondeur uniforme, les courants produits par des forces

locales (la poussée du vent et les gradients de pression). En s'appuyant sur ce modèle et en appliquant une technique statistique multivariée au domaine des fréquences, on démontre que les gradients de pression interne mesurés par les chaînes de thermistances n'ont qu'une incidence minime sur la dynamique des sytèmes à l'étude (bien que la variance observée puisse être en grande partie liée à ces gradients de faible étendue) et que le modèle des forces locales (le frottement du vent à la surface de l'eau et les gradients de pression en profondeur créés par les montées de niveau d'eau dues au vent) expliquent quelques-uns des rapports qui ont été observés entre les vents et les courants. On a également découvert des preuves confirmant que le vent soufflant dans un bassin fermé engendre des tourbillons jumeaux tournant en sens contraire l'un par rapport à l'autre. Bon nombre des caractéristiques de la circulation qui ont été observée, y compris l'évolution saisonnière, peuvent être reliées au rôle de la stratification thermique qui régit la répartition verticale des échanges turbulents.

WATER MOVEMENTS AT A MID-CENTRAL BASIN SITE

INTRODUCTION

The joint experiments of 1979 and 1980 were planned with the advice of chemists, biologists and physicists. Responsibility for the documentation of basin-scale circulations was borne by the Great Lakes Environmental Research Laboratory (NOAA) at Ann Arbor, Michigan (Saylor and Miller, 1986, this volume), while the National Water Research Institute (Environment Canada) at Burlington, Ontario undertook more detailed studies both nearshore and in the open lake. On the advice of participants in Project Hypo (Burns and Ross, 1972), we selected a mid-basin site located approximately halfway between Cleveland, Ohio and Erieau, Ontario (Figure 1). This zone was thought to have relatively homogeneous physical and biochemical characteristics and to be representative of the main offshore portion of the Central Basin where late summer anoxia of the bottom water is frequently observed. An array of current meters, thermistor chains, and meteorological buoys was centred on a point 41 50.5'N by 81 51.0'W, a position designated as Station 27. Measurements were extended both north and south to the shores of the lake. On the south shore near Cleveland, instruments were placed to provide information on the climatology of coastal currents, information useful in evaluating the impacts of effluents introduced near

Cleveland on the rest of the lake. On the north shore of the basin, efforts were made to document the upwelling thought to occur there from time to time(Boyce and Chiocchio, 1986). Information from moored instruments was supplemented by data collected from the ship anchored at Station 27 during three intervals in 1979 and one in 1980. The ship data included profiles of temperature, light transmission, subsurface irradiance, dissolved oxygen and other chemical species (Robertson and Boyce, 1986). Clusters of drogues were tracked by radar from the anchored vessel (Sanderson, 1986, this volume). A major goal of this complex experiment was to study locally acting physical and biochemical processes in a region where they would be most isolated from changes produced by large scale transport and mixing of heat and materials from the nearshore zones.

We wish to examine the extent to which the data supports the hypothesis that the currents depend on wind stress (directly in the upper mixed layer, and indirectly elsewhere due to the pressure gradients caused by wind set-up), internal pressure gradients caused by horizontal variations in the density field, and coriolis force due to the rotation of the earth. Hypolimnion currents are expected to depend strongly on all these factors and this study will focus particularly on them.

SPECTRA AND CROSS-SPECTRA OF CURRENTS IN MID-BASIN

Data from recording current meters form the mainstay of this discussion. With the exception of the MCATS and the GVAPS system (to be described later), these were all of the moving rotor type. They were placed at the locations shown in Figure 1a & b with a maximum of four current meters distributed between a depth of 10 metres and the bottom.

Each successful current meter deployment yields a vector time series comprising a sequence of quadruplets - time, north component of velocity, east componment of velocity, and temperature. The technique of spectral and cross-spectral analysis allows one to make quantitative statements about the distribution of horizontal kinetic energy among a sequence of non-overlapping contiguous frequency bands, and to explore the extent to which motions within each of the bands are linearly correlated over the distances separating the current meters. The technique is valid when the records are long enough and sufficiently sampled to contain an adequate representation of all the imporant (energetic) frequencies, and when the energy in each of the frequency bands is distributed uniformly in time through the record. None of these requirements can be met unequivocally in the practical analysis of Lake Erie data and some care must be taken in the interpretation of the results.

The spectral analysis routine is an adaptation of the Blackman-Tukey mean-lagged-product algorithm. The raw spectral

estimates are smoothed by a Hanning filter and the reported estimates carry at least 20 degrees of freedom. The standard error of a single spectral estimate is 32% before smoothing (Otnes and Enochson, 1972).

We can identify several seasons in the climate of water movements in the Central Basin, the build-up of stratification, the summer stratified period, the breakdown of stratification, and finally the unstratified winter period. Not all of these are of equal interest and we have concentrated on the summer stratified period when oxygen concentrations become low in the bottom waters. We have analysed a sequence of 30 day periods representative of the seasonal changes in the lake and our interest in them:

mid-June to mid-July, 1979 -- early part of stratified season

mid-July to mid-August, 1979 -- mid summer

mid_August to mid-September, 1979 -- late part of stratified season

mid-September to mid-October, 1979 -- breakdown of stratification

mid-November to mid-December, 1979 -- early winter (no ice cover)

mid-February to mid-March, 1980 -- late winter (ice-covered)

August 1 to August 30, 1980 -- late part of stratified season

Figure 2 shows kinetic energy spectra of currents at the 10m and 20 m depth. This general form is typical of currents in mid-basin from June through September. Between frequencies of 0.005 cph and 0.250 cph the energy spectrum decreases with frequency with the exception of a marked peak centred on the local inertial frequency extending from 0.042 cph (24 hr period) to 0.125 cph (8 hr period). This peak contains energies at some of the major resonances of the basin associated with free surface and internal seiches, and pure inertial motions. These will be discussed in more detail below. Spectra fall naturally into three frequency bands; Band A comprising frequencies less than those of the resonance band, frequencies between 0.0104 cph (96 hr) and 0.042 cph (24 hr), band B, the resonance band, between 0.042 cph

(24 hr) and 0.125 cph (8 hr), and band C between 0.125 cph and 0.250 cph (4 hr). The low frequency limit of band A is the limit at which reliable spectral estimates can be formed from a record 30 days long. The upper limit of band C is chosen arbitrarily at a frequency high enough to include the dominant portion of the kinetic energy. In the preliminary discussion of this and other 30 day records we shall examine the distribution of energy within these frequency bands and their spatial coherences in both vertical and horizontal dimensions.

Band averaging obscures all detail within the band but confers a welcome simplicity to an otherwise complicated task. The standard errors of the spectral estimates are reduced by band averaging to 11% for Band A, 7% for Band B, and 5% for Band C (Otnes and Enochson, 1972).

In choosing a figure of merit for the coherence between two vector series we have selected one half the square root of the trace of the covariance matrix, which we shall call averaged coherence. This figure is invariant to rotations of coordinate systems (Calman 1978). The standard error of the estimate of averaged coherence is of order 5% (Otnes and Enochsen, 1972).

Band Averaged Spectra.

Figure 3 provides a graphical summary of the

band-averaged spectra and cross spectra for selected, non-overlapping 30 day periods from June 1979 to March 1980. Spectral amplitudes are presented not as energy densities but as rms velocity scales representing the variance within each of the three bands. These numbers are suitable velocity scales for motions within each of the bands.

The current meter spectra from June through September (first three episodes) are all dominated by Band B peaks, particularly the records from the 15m instruments during the July - August period. This last period is depicted in Figure 2. Within Band B, clockwise motion predominates. The resonant peak is not as obvious in the remaining spectra; from September onwards, circularly polarized inertial period motion is replaced by linearly polarized free-surface seiching. The spectrum for 15 m currents during the September - October period is the result of aliasing surface wave orbital motion via the rectifying properties of a savonius rotor. The band-averaged spectra for February - March, 1980 show roughly equal amounts of energy in Band A and Band B suggesting that the nearly total ice-cover further suppresses the seiching motion.

Horizontal Coherences.

Figure 3 shows horizontal coherences representative of the nominal 10 km by 10 km mid-basin array. When the coherence

between two scalar quantities is less than 0.5, less than 25% of the variance (energy) can be explained by a linear relation between the variables. While the relationship for vector time series is more complex, we retain the value of average horizontal coherence (defined earlier) of 0.50 as the boundary of energetically significant coherence. At the 10 m depth, the horizontal currents are strongly coherent through Bands A and B, less coherent in Band C. The pattern at 20 m depth is similar; the coherences are generally slightly less. Within the 10 km by 10 km array, horizontal phase angles in Bands A and B are effectively zero.

One expects that the averaged horizontal coherence ought to correlate inversely with separation distance between current meters. To test this hypothesis, linear regressions of averaged horizontal coherence on separation distance were computed. When the correlation coefficient of this regression had an absolute value greater than 0.4, the regression line was used to estimate the separation distance at which the coherence reduced to 0.50. This distance serves as a rough length scale for energetically significant coherence (see Table 1).

The table shows significant coherence in bands A and B over many tens of km in the summer months, becoming smaller in the fall. A length scale for Band C could not be determined in 1979, but in 1980, when the minimum current meter separation was

reduced to 3.0 km, the length scale was estimated to be 8 km.

FORCING FUNCTIONS; WIND STRESS AND INTERNAL PRESSURE GRADIENTS

Wind Stress

The distribution in time and space of wind stress has been discussed earlier in the papers of Chapter 2 (see Hamblin, Schertzer et al., 1986, this volume) as has the seasonal build-up and decay of thermal stratification. We shall study the meteorological-buoy wind data collected as close as possible to the central station in the mid-basin array. Root mean square wind speeds in the three bands are presented in Figure 3 (analogous to the current speeds also in Figure 3). The seasonal trend from early summer to late fall is for increased speeds in Band A. The dominance of Band A reflects the dominance of storm events with time-scales greater than a day. During the late fall and winter, data is available at shore stations only. Extrapolation of this data to mid-lake is complicated by the necessity of employing empirical land-water wind ratios (Schwab and Morton, 1985); such an interpolation would be indicative only of the gross, low frequency aspects of the local wind field. We have assembled an average value of the shore-based winds for the winter months for approximate evaluation of the coupling between winds and currents during the winter but we do not present the rms speeds in Figure 3.

During the stratified season, the wind stress directly affects the upper mixed layer while the wind set-up creates surface pressure gradients that are felt throughout the water column. In principle, the pressure gradients can be measured in mid basin by an array of sensitive bottom-mounted water-level gauges. This was attempted in both 1979 and 1980, and Hamblin has employed this data to verify his storm-surge model (Hamblin, 1986, this issue). Since the wind set-up is achieved within a few hours of the onset of a wind event, the surface pressure gradients are very tightly coupled to the wind stress vector, and the latter serves as a primary independent variable.

Internal Pressure Gradients: the Temperature Field.

A description of the seasonal thermal structure of Lake Erie's Central Basin is provided by Schertzer et al (1986, this volume). Winds blowing over a stratified basin cause warm surface water to leave the upwind shore and to accumulate on the downwind shore. The force acting to restore this imbalance and return the surfaces of constant density to their equilibrium level position takes the form of internal pressure gradients. In Figure 4 is shown the topography of the Central Basin thermocline computed from temperature profiles collected during six monitor cruises. Each cruise spans a time interval of about five days, long enough to raise some questions about the synopticity of the results since the timescale of significant adjustment of the density

field towards equilibirium is of the order of two days, and the energetic periods in the wind-forcing spectrum are of the order of a few days, as well. Nevertheless, on four of the six cruises, the observed trend is for a deeper thermocline in the southeastern part of the basin as we would expect from the direction of the prevailing winds. The diagrams indicate that the slope of the thermocline is small in the region of the offshore array (marked on the diagram), of the order of .0001 (10 cm per km). Taking a typical density contrast between the epilimnion and the hypolimnion to be 1.0 kg.m**3, the above slope is dynamically equivalent to a horizontal force acting on the hypolimnion water of 10**-06 n/m**3. The surface pressure gradient force acting over a 23 m water column and set up by a 0.1 n/m**2 wind stress (typical value for significant meteorological event) is of the order of 10**-06 n/m**3 as well, suggesting that the internal pressure gradient force may be significant in the lower layer.

During both the 1979 and 1980 experiments we operated horizontal arrays of three and four thermistor chains, respectively, grouped near the main cluster of current meters. The horizontal separation between thermistor chains was of the order of 10 km. In principle it is possible to estimate isotherm slopes and internal pressure gradients from a minimum of three chains. In practice, the accuracy of the result depends on the horizontal scales over which the thermocline topography varies significantly vis-a-vis the horizontal separation of the

instruments, the uncertainty in the vertical positioning of the instruments, and the resolving power of the vertical array of thermistors. With regard to the vertical positioning, it must be noted that some of the chains had to be remoored when it was discovered that they were too short to allow proper freeboard to the instrument buoy. There is also a possibility that over a span of time the anchors slowly settled deeper into the mud. Several times during the summer of 1979, the vessel ADVENT conducted a temperature survey in the immediate vicinity of the mid basin array. Fourteen temperature profiles were collected over a period of 5 - 6 hours, with the average horizontal separation being less than five km. This data, when processed identically to that collected with the thermistor chains, provides a limited check on the performance of the chains (see below).

For both the thermistor chain data and the temperature profiles collected from ADVENT, the variable computed first is a vertical integral of the density field, from the surface to a reference depth below the surface (in this case 21 m) in the vertically mixed hypolimnion region. The horizontal gradient of this variable, multiplied by the gravitational acceleration, g, is the required estimate of internal pressure gradient at the reference level. Removing the means and linear trends from the two components of the estimated gradient should help to reduce, if not eliminate, the errors due to positioning of the

instruments. The estimated gradient, with means and trends removed, is now filtered to remove all periods less than 36 hours. The smoothed, low frequency values of the observed wind stress are converted to estimates of the surface pressure gradient assuming a steady setup in opposition to the wind. The thickness of the entire water column is taken to be 23 m. It is found that the magnitudes of the estimates of the low frequency (Band A) surface and internal pressure gradients acting on the hypolimnion are comparable.

Thermocline mapping cruises

A measure of the ability of the horizontal array of thermistor strings to sample the internal presssure field is provided by an examination of the "thermocline mapping cruises" mentioned above. In Figure 5 the isopleths of the internal pressure field at a depth of 21 m below the surface, expressed in pascals (newtons/m**2), are sketched over a horizontal area that includes the mid-basin array of current meter moorings and thermistor strings for each of 5 cruises (July 16, 3 August, 8 August, 16 August, and 27 August, 1979). The locations of the three thermistor strings used to form the time series representation of the internal pressure gradient are marked. The bias of the array to the north-south or cross-lake direction should be noted. For each of the cruises, the internal pressure gradient estimated from the thermistor string data is marked on the plot by an arrow

pointing in the direction of the internal pressure gradient force (from high to low pressure) and the length of the arrow is equal to the distance required to produce an internal pressure change of 10 pascals, given the estimated gradient. Note too that the estimated gradient is smoothed to yield approximately daily values.

The first two examples (July 16 and August 3) show evidence of an internal pressure field that varies significantly across horizontal scales of less than 5 km and is consequently undersampled by the array of instruments. On August 8, the mapping cruise shows a steep trough between the two southerly instruments superimposed on a more gentle north-south trend. The internal pressure gradient estimated from the thermistor strings matches this trend. Much less small scale variability is found on August 16. The mapping data shows that the assumption that the internal pressure field can be approximated by an interpolation of measurements separated by 10 km is at times in serious error. However, the perturbing small scale features must be highly mobile, propagating through the region as internal waves. Instantaneous estimates of the internal pressure gradient from the array of thermistor strings will be badly aliased by the small scale features, but values averaged over long enough times may retain dynamical significance.

erie2d.man 22/07/86

DYNAMICAL SIGNIFICANCE OF ESTIMATES OF WIND STRESS, INTERNAL PRESSURE GRADIENTS, AND CORIOLIS FORCE ON CENTRAL BASIN BOTTOM CURRENTS IN MIDSUMMER.

An approximate set of equations of motion for the bottom currents can be written

(1a) $du/dt = fv + Fx - ku$

(1b) $dv/dt = -fu + Fy - kv$

Local accelerations are balanced by the pressure gradient force, (Fx, Fy), the coriolis force, (fv, -fu), and a friction force, (-ku, -kv). Similar equations have been propsed by Pollard and Millard (1970) for the wind-driven upper mixed layer. It is assumed that the lateral variations of currents are small. The system resonates at the local inertial (angular) frequency, f. Assuming forcing functions of the form Fx = Xexp(j(wt+&1)), Fy = Yexp(j(wt+&2)), the corresponding solutions to (1a) and (1b) are written

(2a) $u(t) = Hux*exp(j\&ux)*Fx + Huy*exp(j\&uy)*Fy$

(2b) $v(t) = Hvx*exp(j\&vx)*Fx + Hvy*exp(j\&vy)*Fy$

where Hux*exp(j&ux) etc. are complex transfer functions, expressed in terms of the gain H and the phase angle &. Table (2) gives the gains and phases for the four transfer functions at selected frequencies between 0 and twice the local inertial frequency. At low frequencies, the inertia term is small and the force balance is primarily geostrophic (current directed to the right of the applied force). At higher frequencies, above the local inertial frequency, the dynamic balance is mainly between applied forces and acceleration. This simple model will prove to be useful as a diagnostic tool.

Response of bottom currents to winds and internal pressure gradients.

The hypothesis to be tested is that bottom currents respond to the sum of surface and internal pressure gradients and coriolis force. Since surface pressure gradients at time scales greater than a few hours oppose the wind stress, the wind stress is taken as the primary independent variable. This is stated formally:

(3a) $u(t) = U(v(t), wxx(t), wyy(t), pix(t), piy(t)) + zu(t))$

(3b) $v(t) = V(u(t), wxx(t), wyy(t), pix(t), piy(t)) + zv(t))$

wxx(t) and wyy(t) are the two components of wind stress, pix(t) and piy(t) are the two components of internal pressure gradient, and zu(t) and zv(t) represent the motions that are not related to the independent variables. The independent variables are correlated among themselves (the internal pressure gradients arise from wind-driven water motions, for example), so that simple cross-correlations between an independent variable and a dependent variable may not reveal the true interconnection.

The technique used to study the relationship is that applied to describe linear systems with multiple inputs in the frequency domain (Otnes and Enochson, 1972) (Boyce, 1986). The various steps and end products of this computation are described:

1) Concurrent hourly-sampled time series of all variables are assembled for the time period under investigation. Means and linear trends are removed and each series is normalized to unit variance.

2) Frequency bands of interest are defined and the co- and cross-spectra between all pairs of variables are estimated for each frequency band and stored as a complex-valued matrix. The dependent variable occupies the first row and column.

3) A multiple coherence is estimated for each frequency band from the elements of the cross-spectral matrix. This

coherence is a measure of the portion of the variance of the dependent variable in the frequency band that can be associated with a linear function of the independent variables.

4) Transfer functions (gain and phase) relating the dependent variable to the independent variables are computed together with estimates of their confidence limits. The transfer functions describe the optimum linear relation between the dependent variable and the independent variables in the frequency domain. Because of the normalization of all variables to unit variance, the gains of the transfer functions are of order 1. The relative values of the gains serve to rank the variables in order of importance.

5) Partial coherence between the dependent variable and an independent variable is the residual coherence after removing the effects of the relation of the chosen independent variable to the other independent variables. The partial coherence between u(t) and pix(t) is the coherence between u(t) and the variable pix'(t) that is formed after subtracting from pix(t) the least-square-error linear relation between pix(t) and the variables wxx(t),wyy(t), and v(t).

Table (3a) is the output from the program described above for the period 15 July to 15 August, 1979. The dependent variable is the cross-lake component of current at 19m depth at station

27. This location is in the middle of the offshore array and within the hypolimnion. Independent variables are the along-lake component of velocity, the two components of wind stress, and the two components of internal pressure gradient estimated from the surrounding thermistor chains. Linear trends are removed from the internal pressure gradient components. Means are subtracted from all variables.

Empirical estimates of the 95% confidence limits for the multiple coherence function with comparable degrees of freedom show that multiple coherences greater than 0.05 are significant. Values of multiple coherence greater than 0.200 are attained in the lowest five frequency bands of Table (3a), corresponding roughly to Bands A and B defined previously and decrease to values near the the significance level at higher frequencies. With the exception of the zero frequency band, the transfer function between the v component and the u component of velocity is the largest of all in these five bands and the phase angle denotes clockwise rotation of the velocity vector. The dominant effects of the earth's rotation are seen in both the transfer function and the partial coherence between the two velocity components. Bearing in mind that the wind stress is in the opposite direction to the estimated surface pressure gradient, the phase angles between the wind stress and the current component are close to those of the simple model at frequencies less than the inertial frequency. The phase shift exhibited by

the model as the frequencies change from lower to higher than the inertial frequency is not repeated in the data (see discussion below). The transfer functions between the current component and the internal pressure gradient are significant at the 95% level near the inertial frequency. Both transfer functions bear the same phase relationship to the v component of velocity; this is not compatible with the model. Examination of the power spectra of the two internal pressure components shows approximately equal energies in each frequency band and they are strongly correlated, one with the other. The estimate of the internal pressure gradient has assumed that the thermocline displaces as a plane in the vicinity of the thermistor arrays. This does not allow for any wave propagation effects that would imply different phase relationships at different frequencies. Rather than impose a linear relationship among the measured internal pressure terms, the optimum least-square-error relationship can be determined statistically from the routine described above. In this case the independent variable list contains as before a current component and the two components of wind stress, but also includes the three pressure estimates, one from each of the thermistor arrays. The multiple coherences in this computation (Table 3b) do not differ significantly from those obtained using the pressure gradient estimate (imposed linear relation among the individual pressure estimates). A third computation in which only the wind stress components and the other velocity component are retained as independent variables yields multiple coherences that are

slightly, but significantly (at the 95% level) lower than the previous values in the frequency bands near the inertial frequency (Table 3c).

In 1980, four thermistor strings were operated in the Central Basin array. An estimate of the internal pressure gradient was formed by the least-square-error fit of a plane through the four observed points. The statistical computations were performed first on the set of variables comprising the wind stress components, the internal pressure gradient components, and the other velocity component. Then the calculations were redone, dropping the internal pressure gradient components. Unlike the computations for 1979, the multiple coherences obtained excluding the internal pressure gradient are significantly the larger of the two. Examining the thermistor string records themselves suggests that the instrument to the south of the array may represent a somewhat different regime. The third version of the routine was performed carrying the three most northerly observed pressures as independent variables in addition to the wind stress components and the velocity component. The multiple coherences differ only slightly, and not significantly, from those calculated using the internal pressure gradient estimates.

Thus in 1979, the internal pressure field as sampled by the three thermistor arrays, is dynamically significant, but only marginally so, although the calculated phases do not fit the

simple model. In 1980, the temperature field appears to be less homogeneous; with the same spacing, the sampling is inadequate to resolve a spatially coherent pattern. In all cases the partial coherence between currents and pressure gradient terms is small, indicating that the wind stress is by far the dominant forcing variable at low frequencies.

RESPONSE OF CURRENTS AT 10, 15, AND 20M DEPTHS TO WINDS; ALL SEASONS.

The analysis developed for assessing the response of currents to wind stress and the internal pressure gradient is now applied to current meter data from 10, 15, and 20 m depths over the entire 1979 measurement period. Taking the components of current as the dependent variables, one at a time, the independent variables are the two components of wind stress, and the other component of current. The outputs of the analysis are the multiple coherence that measures the proportion of the total variance of the current signal that can be be associated with a linear combination of the independent variables in each frequency band, and the transfer functions (gains and phase angles plus confidence limits).

Multiple coherences (see Table 3c for an example) at frequencies higher that 0.1 cph approach the significance at all depths and at all times as was noted for the midsummer bottom

currents in the preceeding paragraphs. This frequency may then be considered as a high frequency cutoff for deterministic motion in the Central Basin. Band C may be viewed as large scale turbulence.

It was noted that the evolution of the phase angles between the wind stress components and the current components as the frequency progressed from zero through the inertial frequency did not agree with the output of the simple model to single frequency inputs. To investigate this behaviour, a program was written to solve equations 1a and 1b numerically, and the observed wind record shifted by 180 degrees was used as input. The output, assumed to behave like bottom currents driven by surface pressure gradients, for the mid-July to mid-August period is shown in Table 4. This should be compared with Table 3c. It will be seen that the progression of phase angle of the model matches closely that of the observations. On the other hand, the response of the numerical model to single-frequency inputs is exactly that of Table 2. The two approaches agree at low frequencies, and the discrepancy has obviously to do with the spectrum of the wind forcing. Table 4 may be viewed as the signature of the simple, locally-forced theoretical model.

The spectrum of local winds shows the greatest energies at periods between 50 and 100 hours (0.01 to 0.02 cph). This input will be well represented by the band centred on 0.025 cph

in the calculations described above. For near-surface motion, directly driven by the wind stress, the model indicates that the y-component of current will lead the x-component of wind stress by 0.5 cycles and the y-component of wind stress by 0.25 cycles (see Table 2). For bottom currents driven by the surface pressure gradient, the phases will be shifted by 0.5 cycles. The phase angles then are indicative of the flow regime vis-a-vis the local forcing. In Table 5 we present a summary of calculations identical to those used to prepare Table 3c but extended to 5 measurement periods and three depths.

The multiple coherence squared values are a measure of the success of the presumed linear relation between the y-component of current and three independent variables, the x-component of current and the the two components of wind stress. These values are largest during the mid-July to mid-August period; they become small in the two autumn months.

The phase between the two components of current at all depths is close to the value -0.25 cycles expected for circularly polarized, positively rotating motion from mid-May through to mid-September, but in the final period (September-October) it shifts to nearly 0.5 cycles, a value associated with rectilinear motion.

With two exceptions, both occurring at 15 m depth, the

phase relationship between the y or cross-lake component of current and the the along-lake or x component of wind stress fits the model, either as a surface-driven response or a pressure-gradient driven, bottom-layer response. The 15m depth appears to be one of transition between the two regimes; this feature is discussed more fully elsewhere in this volume (Boyce, 1986 __). Concerning this phase relationship then, during all months the 10 m depth belongs to a surface-driven regime. With the exception of the two "maverick" 15m records, the observations at 15 and 20 m fit a bottom, pressure gradient-driven regime. In the final period, September-October, all depths correspond to the surface-driven regime. This development must reflect the extension of the wind-mixed layer to the bottom of the lake once the stratification has disappeared.

The phase relationship between the y-component of wind stress and the y-component of current is less-easiliy interpreted. Four of the 15 phase angles can be interpreted as the bottom or pressure gradient driven regime, but the phases of the remaining examples are such that the current component directly opposes the wind stress component.

Treating the x-component of current as a dependent variable yields similar results. Concerning the phase relationship between current components and wind stress components, the phase between the x-component of current and the

y-component of wind stress can be fitted to the model of locally driven currents, whereas the relation between the x-component of current and the x-component of wind stress contains a preponderance of opposing phases.

A possible interpretation of these results is that they give evidence of two coexisting wind-driven regimes. The first regime, described by equations (1a) and (1b), is that of currents driven locally by either the direct action of the wind or the pressure gradient caused by wind set-up. This regime would obtain only when the quasi-static wind set-up could be achieved in a small fraction of the inertial period. The second flow regime is the one giving rise to basin scale gyral motions in closed basins of variable depth; water moves downwind in the shallow zones and upwind in the deep (Bennett, 1974). The observations contain the deep water response. When the stratification is very pronounced, the first regime predominates.

SUMMARY AND CONCLUSIONS.

Current and wind spectra are conveniently studied in terms of three main frequency bands. A low frequency band (Band A) extending from the lowest resolvable frequency to the diurnal frequency, a resonant frequency band including the inertial and first-mode seiching frequencies (Band B), and a high frequency band extending from 0.125 to 0.250 cph (Band C).

A striking feature of the currents observed in the stratified period mid-July to mid-August are the very large inertial period motions at the 15 m depth. These are the largest of all observed currents. A separate paper (Boyce, 1986 __) in this issue deals specifically with this feature.

Motions in Bands A and B cohere horizontally over tens of kilometres as opposed to a few km for Band C. Observed horizontal coherences are largest in mid-summer (stratified) and become smaller in the fall (unstratified). Within the mid-basin array, phase angles for motions in Bands A and B are effectively zero.

Thermocline topography derived from surveillance cruise data shows the mid-basin array to be located in a zone of relatively flat topography. Narrow zones of upwelling (northwest shore) and downwelling (southeast shore) are observed consistent with the prevailing winds. Mid-basin internal pressure gradients are nevertheless estimated to be at times dynamically significant to flows in the hyplolimnion. Time-series of internal pressure gradients in the hypolimnion are estimated from self-recording thermistor strings spaced roughly 10 km apart. Root mean square values of these gradients are comparable to estimated surface pressure gradients due to wind set-up. Limited comparison of the time series data with detailed mapping of the internal pressure

field obtained from a few densely sampled launch cruises indicates that the 10 km thermistor string spacing seriously undersamples the horizontal variability existing in the temperature field; the time series estimates of internal pressure gradient must be averaged over 24 hours or more to eliminate aliasing by small-scale variations.

Multiple coherence-squared functions, transfer functions (gains and phases) in the frequency domain, together with a simple dynamical model are used to establish the dynamical significance of the estimated internal pressure gradient. In 1979, the internal pressure gradient is marginally significant at low frequencies, in 1980, not at all.

The statisitcal techniques and model mentioned above are applied to an analysis of the relation between currents and the major forcing variable, the local wind stress. The multiple coherence squared function becomes statistically insignificant for all periods and all depths at frequencies higher than 0.10 cph. Motions in Band C are then viewed as large-scale turbulence. The mutliple coherence squared function attains the largest values (0.65) in the mid-July to mid-August period and the smallest values (0.15) in the mid-September to mid-October period.

The portion of the current component variance explained by the optimum linear relation with wind stress is described by

the transfer functions, both gains and phases. The phase angles are most simply interpreted. The phase angle between the two current components is indicative of a clockwise rotating current vector in all measurement periods except the September-October period where the phase angle suggests rectilinear motion. The phase relation between the wind component at right angles to a velocity component shifts by half a cycle with depth. It can be explained in terms of a simple, locally-forced model by assuming that the near surface motions are directly powered by wind stress while the near-bottom motions are powered by the surface pressure gradient arising from wind set-up. The relation between a velocity component and the wind stress component parallel to it does not usually fit the model, and more often than not, the currents oppose the wind stress. This last feature can be interpreted as the offshore signature of the two-gyre mode of wind driven circulation in closed basin first proposed by Bennett (1974).

The unexplained variance in the current signals is typically 50% or more. Sources of this variance are measurement errors, small (horizontal) scale internal pressure gradients, unidentified non-linear mechanisms, bottom topography effects, and large-scale turbulence.

A recurring feature of the entire discussion is the degree to which the currents depend on the thermal

stratification. The role of stratification in producing internal pressure gradients appears to be primarily a small-scale phenomenon, not well resolved by the measurements. On the other hand, the role of stratification in controlling the vertical distribution of turbulence appears very important.

REFERENCES

Bennett, J.R., 1974. On the dynamics of wind-driven lake currents. J. Phys. Oceanogr. 4: 400-414.

Boyce, F.M., 1986. Program PARCOH2: Partial and multiple coherences, transfer functions in the frequency domain. NWRI Internal Report 86-15, 29p.

Boyce, F.M., and F. Chiocchio, 1986a. Near-inertial period currents in Lake Erie at a Central Basin site. J.G.L.R., this volume.

Burns, N.M., and C. Ross, 1972. Project Hypo - an intensive study of the Lake Erie Central Basin hypolimnion and related surface water phenomena. CCIW paper #6. USEPA Tech. Rep. TS-05-71-208-24. 182 pp.

Calman, J., 1978. On the interpretation of ocean current spectra: the kinematics of 3-D vector time series. J Phys. Oceanogr. 8: 627-643.

Chiocchio, F. and F.M. Boyce, 1986. Upwelling on the northwest shore of Lake Erie's Central Basin, 1979 - 1980. NWRI Report (in preparation)

Hamblin, P.F., 1986. Meteorological forcing and water level fluctuations on Lake Erie. J.G.L.R., this volume.

Otnes, R.K., and L. Enochson, 1972. Digital Time Series Analysis. John Wiley and Sons, New York, 455 pp.

Pollard, R.T. and R.C. Millard Jr., 1970. Comparison between observed and simulated wind-generated inertial oscillations. Deep Sea Res. 17: 813-822.

Robertson, D.G. and F.M. Boyce, 1986. Physical and biochemical measurements in central Lake Erie: the anchor station experiments of 1979 and 1980. NWRI Report (in preparation)

Sanderson, B., 1986. Lagrangian kinematics at a mid-Central Basin site in Lake Erie. J.G.L.R., this volume.

Saylor, J.H. and G.S. Miller, 1986. Studies of large-scale currents in Lake Erie, 1979 - 80. J.G.L.R., this volume.

Schwab, D.J. and J.A. Morton, 1984. Estimation of overlake wind speed from overland wind speed: a comparison of three methods. J.G.L.R. 10: 68-72.

TABLE CAPTIONS

Table 1. Estimates of the distance at which horizontal coherence is reduced to 0.5 for motions in Bands A, B, and C (the last for 1980 only). Under "Separations" are the minimum and maximum instrument separation distances in the network of observations.

Table 2. Gain and phase angles for the transfer functions between sinusoidally varying pressure gradient forces and reslulting currents for the equations 1a and 1b. The friction time scale, 1/k, is set to 12 hours, the local inertial frequency is 0.0558 cph (period = 17.9 hours). Phase angles are expressed in cycles and represent the amount the forcing function lags behind the response.

Table 3. a) Multiple coherence, transfer functions, partial coherences describing the relation between the across-lake component of current at 19 m depth and a group of independent variables comprising the along-lake component velocity, two wind stress components, and two internal pressure gradient components. The time interval is from July 15 to August 15, 1979.

b) Similar to Table 3a except that the two internal pressure gradient components are replace by three pressures.

c) Similar to Table 3a except that the internal pressure gradient components have been removed from the list of independent variables.

Table 4. Identical to Table 3c. The velocity signal analysed is a numerical solution of equations 1a and 1b using the July 15 to August 15 wind record to estimate the surface pressure gradient. Results can be compared directly with Table 3c.

Table 5. Multiple coherence squared between the cross-lake component of current and the optimum linear combination of the along-lake component of velocity (Coriolis force), and the two components of wind stress (x - along, y - across). Phase angles (number of cycles by which response LEADS forcing) between the cross-lake component of velocity and the three independent variables.

S indicates the phase relationship is consistent with a surface-driven motion. B indicates that the phase relationship is consistent with a surface pressure gradient driven flow. R indicates that the response is a return flow, moving against the wind. Calculations are performed for three depths and five, month-long episodes. An asterisk (*) indicates that the 95% confidence limits of the phase angle are greater than 0.25 cycles.

TABLE 1.

Interval	Depth (m)	and Band	Separations (km) Min	Max	Length Scale (km)
June/July 79	10	A	5.5	27	37
	10	B	5.5	27	)100
July/Aug 79	10	A	5.5	102	116
	10	B	5.5	102	148
	20	A	5.5	100	122
	20	B	5.5	100	115
Sept/Oct 79	10	A	5.5	20	24
	10	B	5.5	20	n/s
	20	A	5.5	20	31
	20	B	5.5	20	38
August 80	10	A	3.0	10.5	)60
	10	B	3.0	10.5	)30
	10	C	3.0	10.5	8
	20	A	3.0	10.5	)70
	20	B	3.0	10.5	)120
	20	C	3.0	10.5	8

TABLE 2.

Frequency (cph)	Hux $ux	Huy $uy	Hvx $vx	Hvy $vy
0.00	.643 0.0	2.70 0.0	2.70 0.50	.643 0.0
0.025	1.64 0.13	3.23 -.04	3.23 .46	1.64 .13
0.050	5.32 .04	5.74 -.16	5.74 .34	5.32 .04
0.075	3.95 -.17	2.89 -.39	2.89 .11	3.95 -.17
0.100	2.22 -.21	1.23 -.44	1.23 .06	2.22 -.21
0.125	1.57 -.22	0.69 -.46	0.69 .04	1.57 -.22

TABLE 3a

19M CURRENTS 15JULY – 15AUGUST 1979

FREQ CH	COH2M	U HAM/ANG1	WX HAM/ANG2	WY HAM/ANG3	PIX HAM/ANG4	PIY HAM/ANG5	U PCOH21	WX PCOH22	WY PCOH23	PIX PCOH24	PIY PCOH25
0.000	.664	.021	.214	.577 .176	.085 .141	.104 .154	.043 .162	.011	.625	.021	.024 .005
		0.01	-.99	0.00 .05	.50 -.99	0.00 -.99	0.00 -.99	.047	.413	.102	.041 .001
.025	.667	.493	.192	.588 .181	.211 .161	.142 .182	.131 .196	.282	.547	.092	.031 .032
		-.27	.06	-.03 .05	-.35 .14	.15 -.99	.22 -.99	.076	.397	.313	.403 .003
.050	.689	.668	.166	.574 .187	.287 .227	.340 .266	.338 .284	.491	.329	.091	.065 .087
		-.28	.04	-.00 .05	-.31 .15	.25 .14	.25 .16	.292	.356	.335	.309 .012
.075	.643	.635	.173	.462 .188	.225 .323	.506 .430	.516 .352	.464	.136	.034	.126 .114
		-.29	.04	.10 .06	-.24 -.99	.24 .16	.23 .12	.598	.164	.117	.319 .035
.100	.438	.463	.206	.398 .198	.149 .351	.387 .526	.407 .349	.277	.080	.317	.378 .071
		-.29	.07	.22 .08	-.30 -.99	.22 -.99	.21 .16	.293	.254	.113	.002 .029
.125	.107	.119	.248	.235 .202	.141 .321	.145 .489	.159 .332	.024	.034	.024	.012 .012
		-.25	-.99	.24 .16	-.39 -.99	.22 -.99	.22 -.99	.035	.018	.033	.003 .005
.150	.065	.122	.253	.126 .191	.155 .347	.051 .451	.038 .339	.028	.009	.030	.001 .001
		.01	-.99	.15 -.39	-.41 -.99	.15 -.99	.14 -.99	.029	.014	.042	.001 .001
.175	.053	.138	.254	.135 .199	.090 .398	.068 .471	.043 .378	.032	.007	.008	.002 .001
		.02	-.99	.38 -.99	-.43 -.99	-.31 -.99	-.22 -.99	.022	.019	.005	.016 .013
.200	.051	.069	.253	.244 .206	.057 .411	.111 .489	.177 .394	.006	.023	.003	.005 .011
		-.18	-.99	.42 .16	-.40 -.99	-.20 -.99	-.29 -.99	.026	.029	.002	.015 .024
.225	.041	.053	.254	.170 .209	.040 .365	.189 .493	.252 .407	.005	.013	.001	.014 .021
		-.34	-.99	.43 -.99	-.39 -.99	-.28 -.99	-.26 -.99	.030	.011	.000	.001 .012
.250	.018	.044	.257	.180 .203	.026 .366	.077 .485	.017 .422	.003	.005	.001	.002 .000
		.50	-.99	.50 -.99	-.50 -.99	-.50 -.99	-.06 -.99	.016	.002	.000	.005 .003

(1) TRANSFER FUNCTION GAIN (2) 95% CONFIDENCE INTERVAL (±) FOR GAIN

(3) TRANSFER FUNCTION PHASE ANGLE (CYCLES) (4) 95% CONFIDENCE INTERVAL (±) FOR ANGLE

(5) MULTIPLE COHERENCE SQUARED FUNCTION

(6) PARTIAL COHERENCE SQUARED (7) ORDINARY COHERENCE SQUARED

TABLE 3b

DEP VAR S = P41

19M CURRENTS JULY - 15 AUGUST, 1979

FREQ	CONZN	U MAM/ANG1		WX MAM/ANG2		WY MAM/ANG3		P45 MAM/ANG4		P40 MAM/ANG5		P41 MAM/ANG6		U PCOH21	WX PCOH22	WY PCOH23	P45 PCOH24	P40 PCOH25	P41 PCOH26
0.000	.672	.040	.231	.586	.190	.065	.153	.268	1.218	.257	.711	.083	.564	.602	.634	.012	.006	.010	.002
		0.00	-.99	0.00	.05	.50	-.99	.50	-.99	0.00	-.99	0.00	-.99	.047	.413	.002	.000	.000	.000
.025	.676	.496	.206	.597	.194	.213	.173	.300	1.297	.471	.832	.341	.672	.291	.560	.094	.006	.024	.020
		-.27	.07	-.03	.25	-.34	.15	-.44	-.99	.17	-.99	-.19	-.99	.076	.397	.013	.000	.000	.000
.050	.693	.672	.178	.585	.230	.292	.242	.380	1.151	1.065	1.064	.681	.929	.499	.342	.096	.006	.073	.040
		-.28	.04	-.01	.16	-.31	.16	-.24	-.99	.25	.24	-.24	-.99	.292	.356	.035	.000	.002	.001
.075	.637	.644	.186	.479	.204	.230	.348	.461	.538	1.405	1.205	.903	1.145	.472	.133	.027	.009	.097	.051
		-.29	.09	.09	.07	-.26	-.99	-.18	-.99	.24	.16	-.29	-.99	.588	.164	.117	.004	.017	.013
.100	.629	.471	.224	.386	.216	.118	.380	.351	.337	.848	1.173	.761	1.149	.280	.074	.010	.007	.048	.037
		-.29	.08	.22	.09	-.32	-.99	-.21	.20	.21	-.99	-.30	-.99	.293	.254	.113	-.004	-.005	-.013
.125	.616	.116	.267	.225	.216	.133	.343	.164	.288	.315	.967	.430	.671	.023	.032	.022	.002	.009	.017
		-.25	-.99	.25	.21	-.40	-.99	-.27	-.99	.23	-.99	-.29	-.99	.035	.018	.033	.001	.001	.003
.150	.073	.124	.273	.122	.207	.146	.372	.155	.336	.224	.961	.202	.846	.029	.008	.029	.002	.005	.004
		.02	-.99	.17	-.99	-.42	-.99	-.33	-.99	.26	-.99	-.28	-.99	.029	.014	.042	.028	.004	.006
.175	.055	.140	.275	.155	.215	.185	.430	.345	.328	.077	1.126	.121	1.018	.033	.010	.008	.007	.000	.001
		.02	-.99	.39	-.99	-.42	-.99	-.39	.20	.38	-.99	-.19	-.99	.022	.019	.005	-.105	-.030	-.020
.200	.052	.061	.274	.279	.223	.155	.447	.383	.348	.301	1.171	.153	1.117	.006	.029	.003	.007	.000	.001
		-.08	-.99	.43	.15	-.44	-.99	-.38	.18	-.30	-.99	.15	-.99	.026	.029	.002	.015	.011	.002
.225	.040	.055	.275	.191	.222	.033	.420	.219	.383	.374	1.119	.393	1.163	.105	.016	.001	.002	.011	.008
		-.34	-.99	.42	-.99	-.09	-.99	-.23	-.99	-.30	-.99	.31	-.99	.030	.011	.000	.012	.020	.002
.250	.019	.045	.278	.089	.220	.017	.400	.287	.447	.161	1.069	.324	1.207	.003	.004	.000	.003	.002	.005
		.50	-.99	.50	-.39	-.50	-.99	-.00	-.99	-.50	-.99	.50	-.99	.016	.002	.000	.004	.009	.003

TABLE 3C

VEL 1 = U-COMPONENT
VEL 2 = WX
VEL 3 = WY

19M CURRENTS 15 JULY - 15 AUGUST, 1978

FREQ	COH2N	U MAM/ANG1		WX MAM/ANG2		WY MAM/ANG3		U PCOH21	WX PCOH22	WY PCOH23
0.010	.656	.023	.177	.562	.142	.057	.110	.001	.617	.010
		0.00	-.99	0.00	.04	.50	-.99	.047	.413	.002
.025	.650	.496	.160	.584	.147	.195	.127	.278	.545	.084
		-.27	.05	-.03	.04	-.35	.11	.076	.397	.013
.050	.655	.713	.139	.606	.196	.302	.186	.511	.344	.098
		-.28	.03	-.02	.04	-.34	.11	.292	.356	.035
.075	.586	.697	.142	.486	.163	.211	.275	.507	.124	.028
		-.29	.03	.07	.05	-.32	-.99	.588	.164	.117
.100	.387	.503	.168	.373	.168	.120	.296	.312	.065	.010
		-.30	.05	.22	.07	-.34	-.99	.293	.254	.113
.125	.094	.126	.202	.219	.164	.130	.261	.027	.029	.021
		-.26	-.99	.24	.14	-.39	-.99	.035	.018	.033
.150	.063	.121	.205	.120	.154	.146	.281	.027	.008	.029
		.01	-.99	.15	-.99	-.41	-.99	.029	.014	.042
.175	.044	.138	.207	.144	.161	.087	.324	.032	.009	.008
		.02	-.99	.38	-.99	-.42	-.99	.022	.019	.005
.200	.034	.060	.208	.275	.168	.055	.337	.006	.028	.003
		-.08	-.99	.42	.10	-.41	-.99	.026	.029	.002
.225	.020	.059	.209	.174	.167	.037	.316	.006	.013	.001
		-.33	-.99	.44	.21	-.43	-.99	.038	.011	.000
.250	.007	.046	.210	.077	.164	.025	.300	.003	.003	.001
		.50	-.99	.50	-.99	-.50	-.99	.016	.002	.000

TABLE 4

BOTTOM CURRENTS FROM MODEL
WIND DATA FROM 15 JULY - 15 AUGUST 1979

FREQ	COH2M	HAM/ANG1		HAM/ANG2		HAM/ANG3		PCOH21	PCOH22	PCOH23
		U		WX		WY		U	WX	WY
0.000	.816	.029	.144	.685	.110	.134	.102	.001	.835	.052
		0.00	-.99	0.00	.03	.50	.14	.012	.460	.012
.025	.946	.822	.064	.594	.056	.375	.053	.857	.878	.621
		-.25	.01	-.02	.02	-.28	.02	.103	.439	.026
.050	.986	.913	.028	.453	.027	.302	.036	.979	.874	.731
		-.25	.00	-.02	.01	-.26	.02	.588	.365	.044
.075	.989	.917	.025	.285	.024	.178	.043	.986	.644	.456
		-.25	.00	-.02	.01	-.26	.04	1.325	.180	.138
.100	.971	.895	.041	.186	.037	.121	.056	.961	.295	.219
		-.25	.01	-.01	.03	-.26	.08	.716	1.093	.298
.125	.921	.853	.075	.147	.065	.112	.046	.877	.234	.316
		-.25	.01	-.01	.07	-.26	.07	2.400	.109	.230
.150	.804	.764	.125	.089	.117	.093	.035	.623	.162	.398
		-.28	.03	-.06	-.99	-.23	.06	3.700	.247	.692
.175	.686	.686	.128	.013	.123	.053	.034	.577	.036	.173
		-.25	.03	-.09	-.99	-.22	.11	.257	.230	.284
.200	.479	.543	.153	.028	.132	.031	.047	.415	.015	.037
		-.25	.05	-.48	-.99	-.23	-.99	.353	.849	.062
.225	.301	.328	.178	.041	.136	.018	.032	.189	.066	.028
		-.29	.09	-.47	-.99	-.24	-.99	.212	.091	.064
.250	.353	.323	.172	.048	.114	.009	.017	.239	.201	.026
		.50	.09	-.50	-.99	-.10	-.99	.137	.145	.016

TABLE 5.

Date	Depth	M Coh2	&vu	&vx		&vy	
16/5 - 14/6	10m	.338	-.17	-.44	S	.49	R
	15m	.463	-.19	-.06	B	-.48	R
	20m	.487	-.18	-.07	B	-.48	R
15/6 - 15/7	10m	.305	-.20	-.42*	S	-.48*	R
	15m	.220	-.23	-.28*		-.20	B
	20m	.359	-.24	-.01	B	-.20	B
15/7 - 15/8	10m	.669	-.23	-.44	S	.46	R
	15m	.642	-.26	-.16*	B	-.29*	B
	20m	.650	-.27	-.03	B	-.35	
15/8 - 15/9	10m	.144	-.13	.45*	S	.46*	R
	15m	.137	-.37	-.30*		-.48	R
	20m	.399	-.26	.02	B	-.39*	R
15/9 - 15/10	10m	.278	.44*	.49	S	-.44	R
	15m	.135	.47	.49	S	-.47*	R
	20m	.129	-.49*	.48	S	.46	R

FIGURE CAPTIONS

Figure 1. Map of Lake Erie showing the placement of current meters, meteorological buoys, thermistor arrays, tide gauges, and cruise tracks for the 1979 (figure 1a) and 1980 (figure 1b) experiments.

Figure 2. Spectra of horizontal currents at Station 27 (mid-array location 41 50' 32" N by 81 50' 56" W) for the interval 12 July to 9 August, 1979. Currents are resolved into clockwise and anticlockwise rotating components. Figures 2a, 2b, and 2c show spectra for the depths 10m, 15m, and 20m respectively.

Figure 3. Representations of band-averaged spectra and cross-spectra among winds and currents in the mid-basin array for the 1979 - 1980 period. Spectra are represented as rms velocities in each of the bands. The 15 m current spectrum in September - October is contaminated by surface wave orbital motions.

Figure 4. Topography of the Central Basin hypolimnion from 1979 surveillance cruise data. The surface described is the top of the lower mixed layer.

Figure5. Internal pressure field at a depth of 21 m formed closely spaced temperature profiles in the mid-basin array. Units of isopleths are pascals. Triangles mark the locations of active thermistor strings. The arrow points in the direction of the internal pressure gradient force deduced from the thermistor string data. The length of the arrow is the distance required to produce a 10 pascal pressure change.

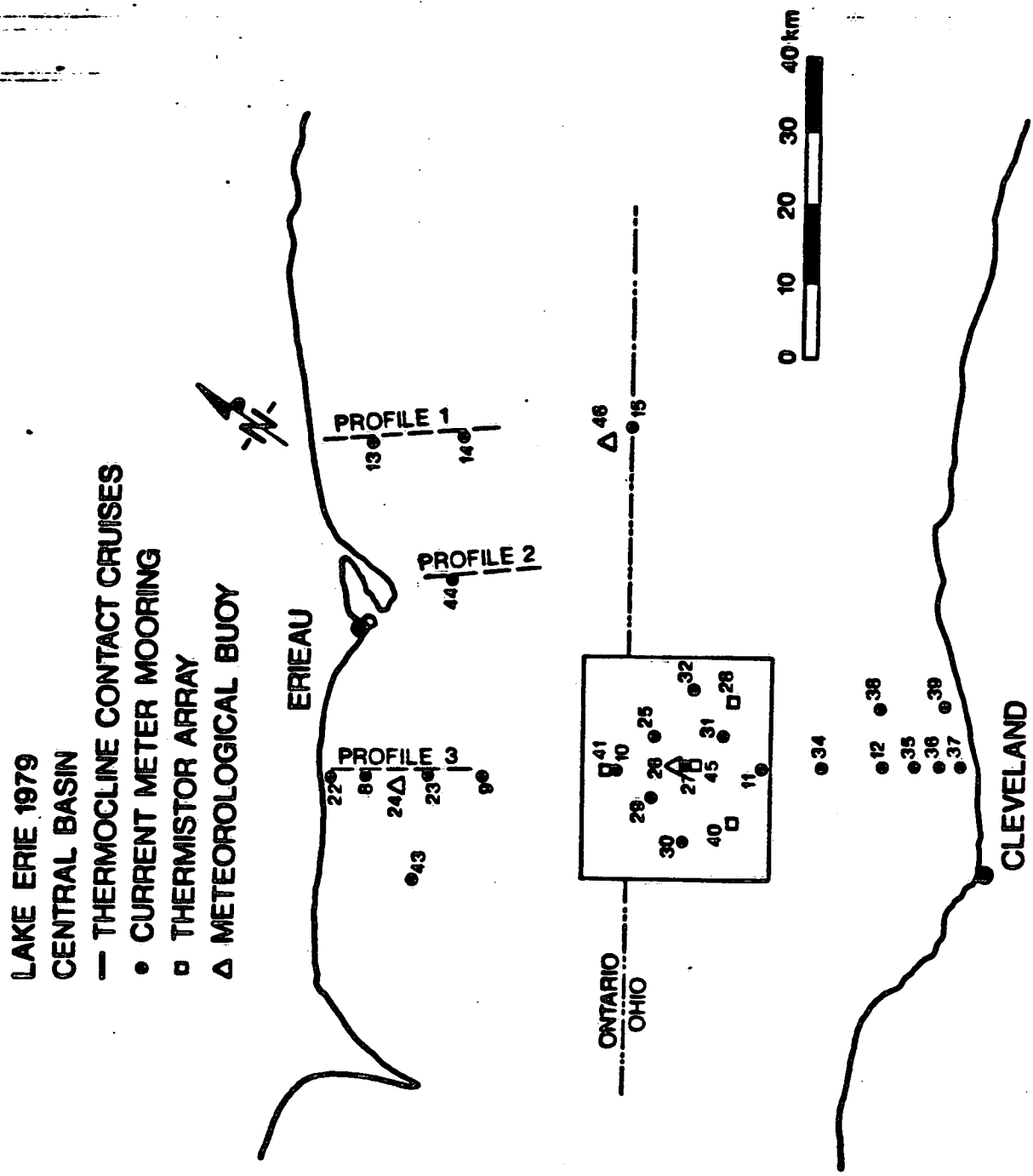
LAKE ERIE 1979
CENTRAL BASIN
— THERMOCLINE CONTACT CRUISES
• CURRENT METER MOORING
▫ THERMISTOR ARRAY
△ METEOROLOGICAL BUOY
PROFILE 1
PROFILE 2
PROFILE 3
ERIEAU
ONTARIO
OHIO
CLEVELAND
0 10 20 30 40 km

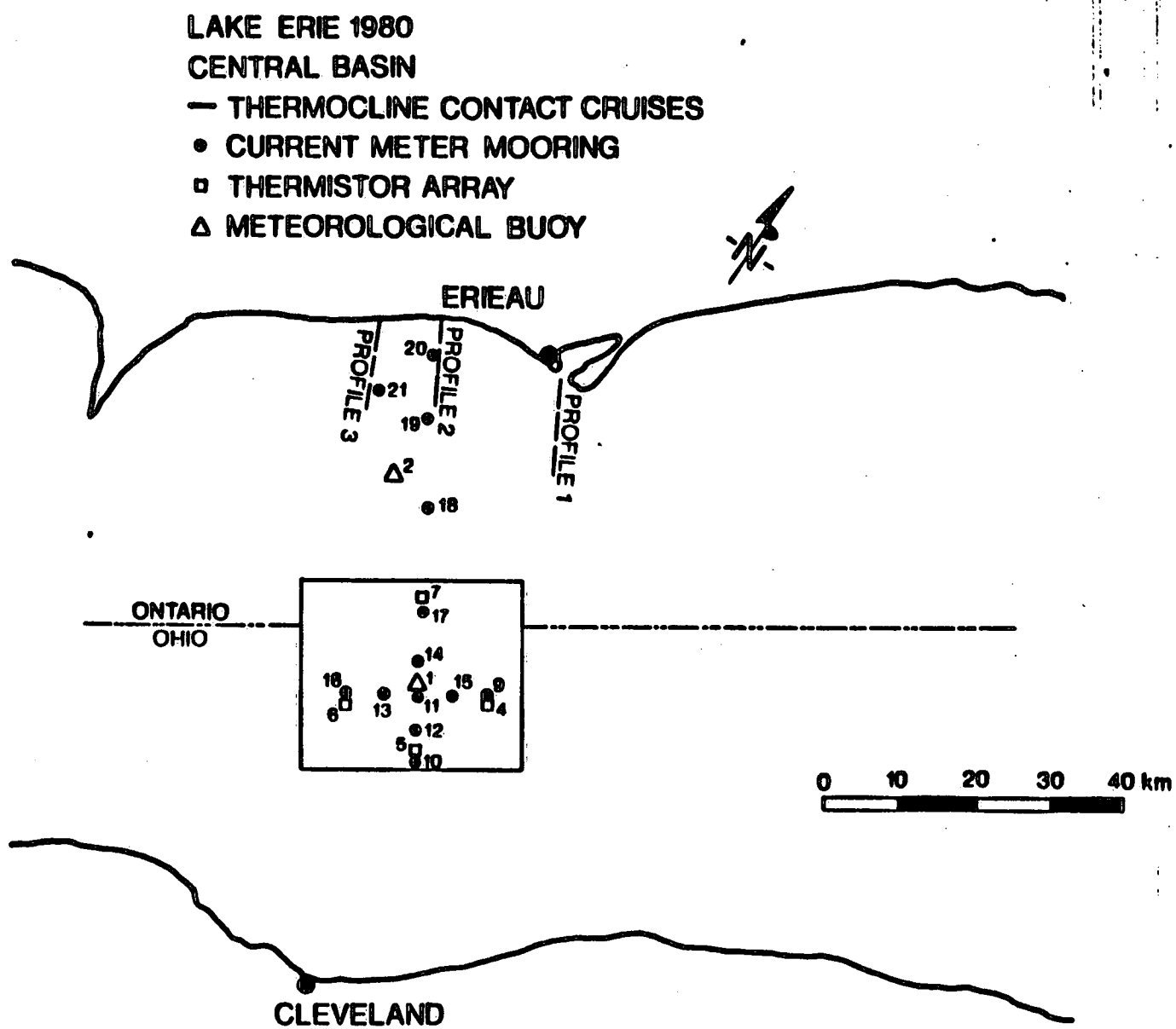
LAKE ERIE 1980
CENTRAL BASIN
— THERMOCLINE CONTACT CRUISES
• CURRENT METER MOORING
▫ THERMISTOR ARRAY
△ METEOROLOGICAL BUOY
ERIEAU
PROFILE 3
PROFILE 2
PROFILE 1
20
21
19
18
ONTARIO
OHIO
7
17
14
16
1
15
9
6
13
11
4
12
5
10
0 10 20 30 40 km
CLEVELAND

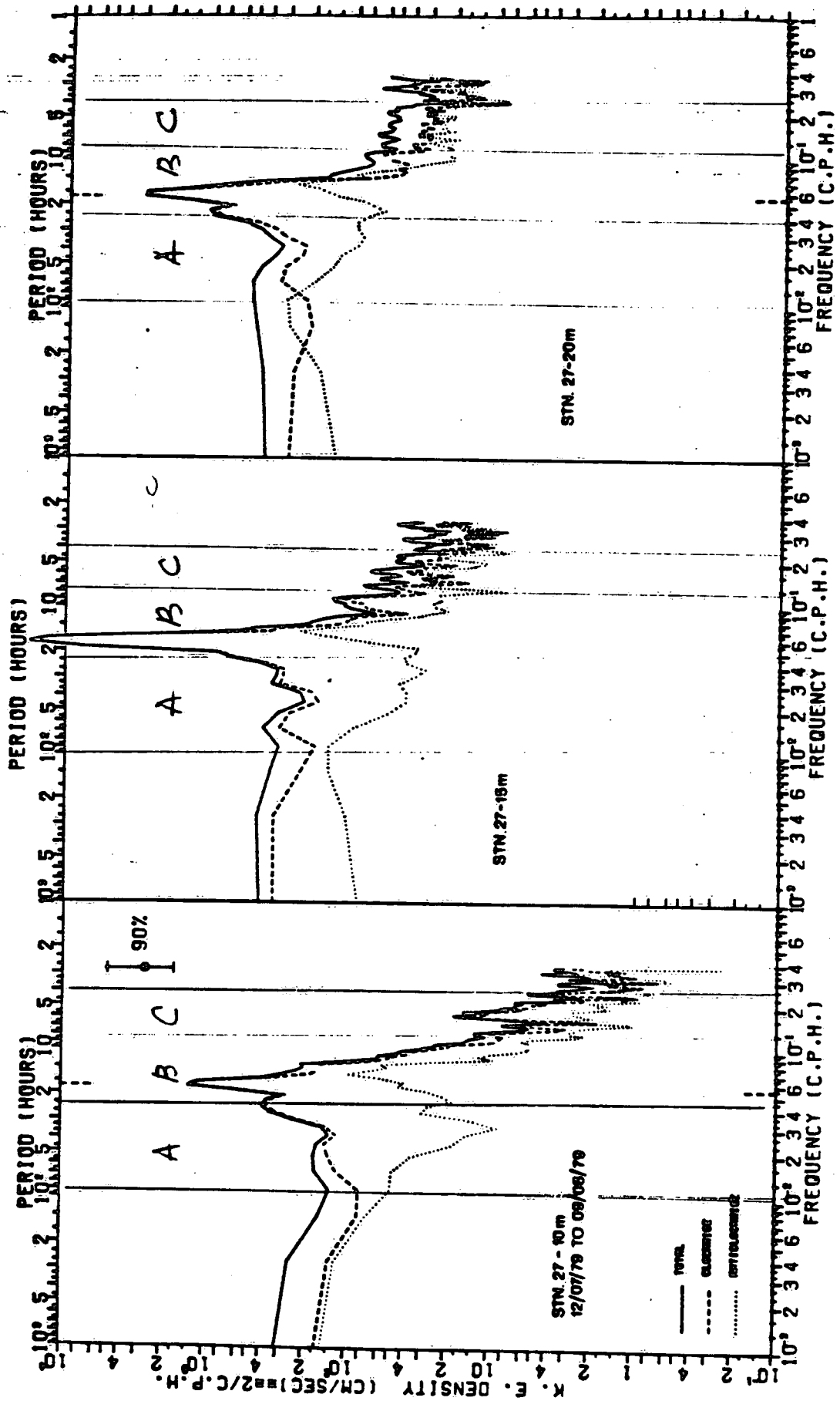
K. E. DENSITY (CM/SEC)²/C.P.H.
PERIOD (HOURS)
FREQUENCY (C.P.H.)
STN. 27-10m
12/07/79 TO 08/08/79
STN. 27-15m
STN. 27-20m
A
B
C
90%

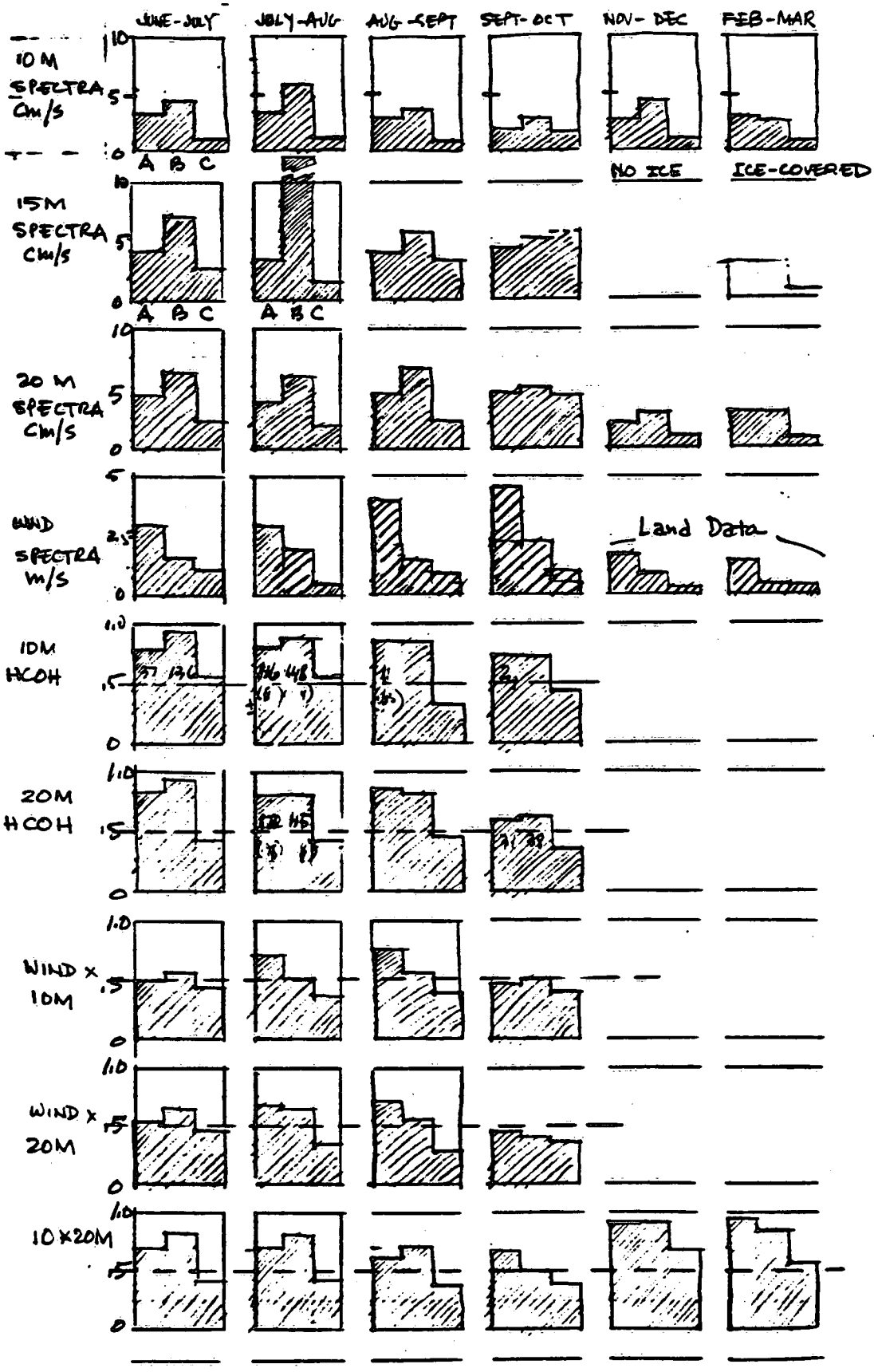
JUNE-JULY
JULY-AUG
AUG-SEPT
SEPT-OCT
NOV-DEC
FEB-MAR
10M SPECTRA CM/S
A B C
NO ICE
ICE-COVERED
15M SPECTRA CM/S
A B C
A B C
20M SPECTRA CM/S
WIND SPECTRA M/S
Land Data
10M HCOH
20M HCOH
WIND X 10M
WIND X 20M
10X20M

FIGURE 3

FIGURE 4

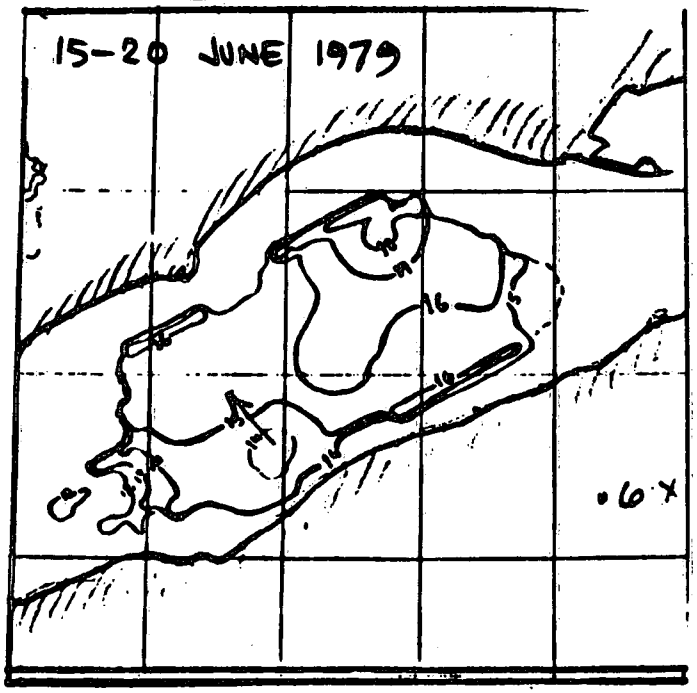
15-20 JUNE 1979
16
•6 X

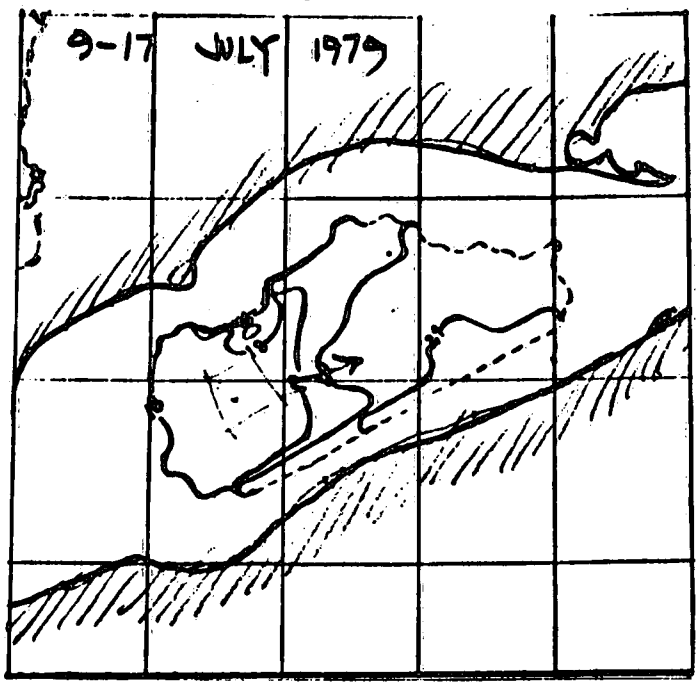
9-17 JULY 1979

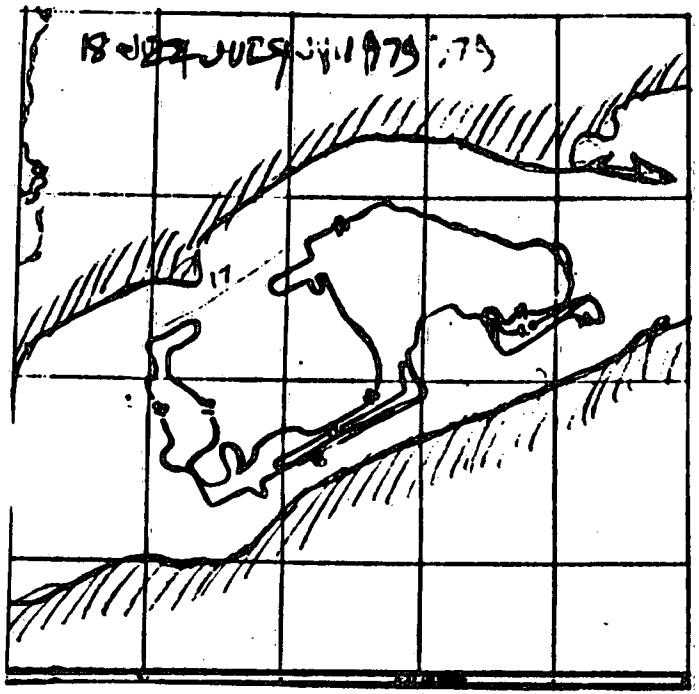
17

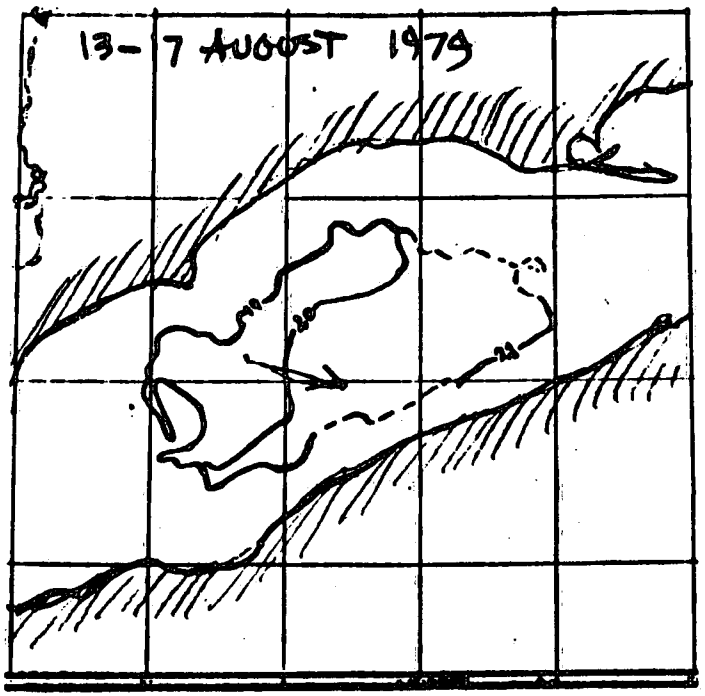
13-17 AUGUST 1979

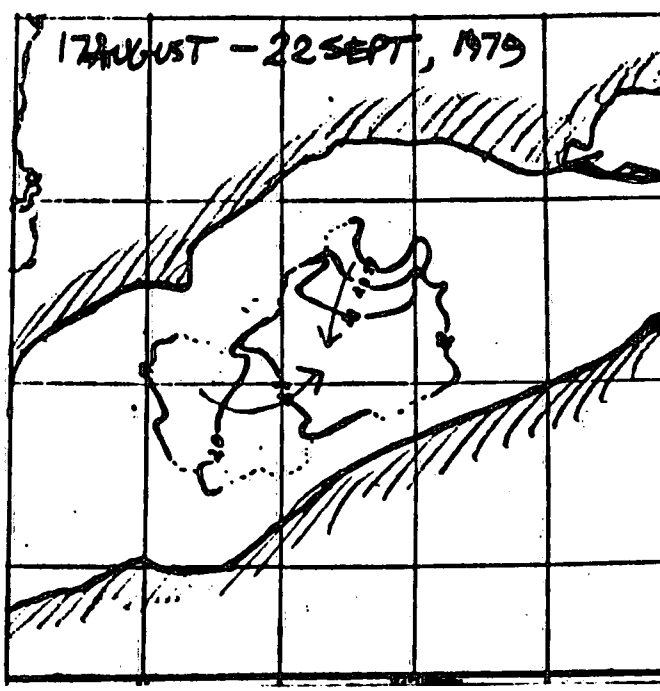
17 AUGUST - 22 SEPT, 1979

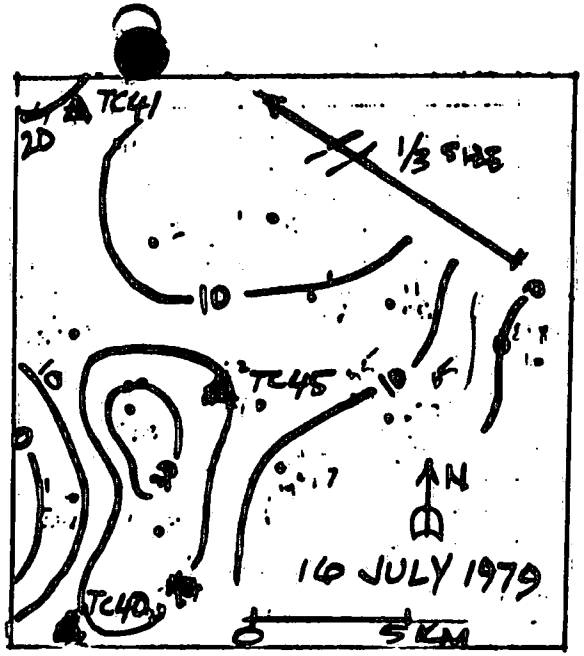
TC41
TC45
TC40
1/3 SHADE
10
N
16 JULY 1979
0
5KM

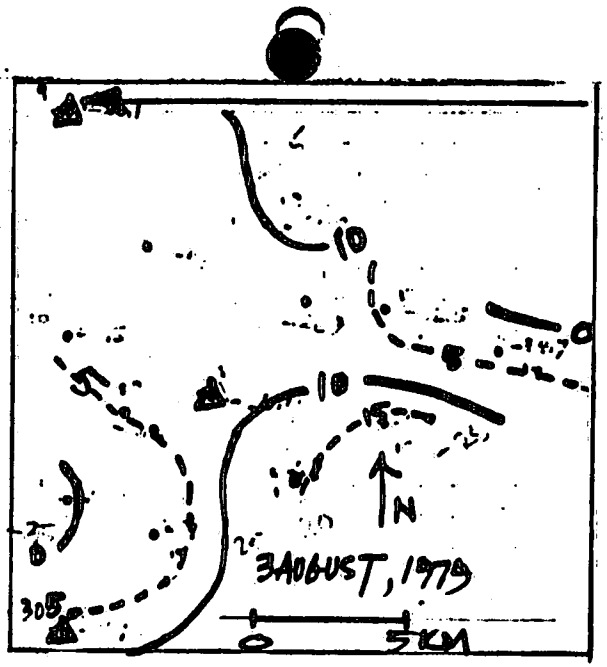
10
N
3 AUGUST, 1979
0
5KM

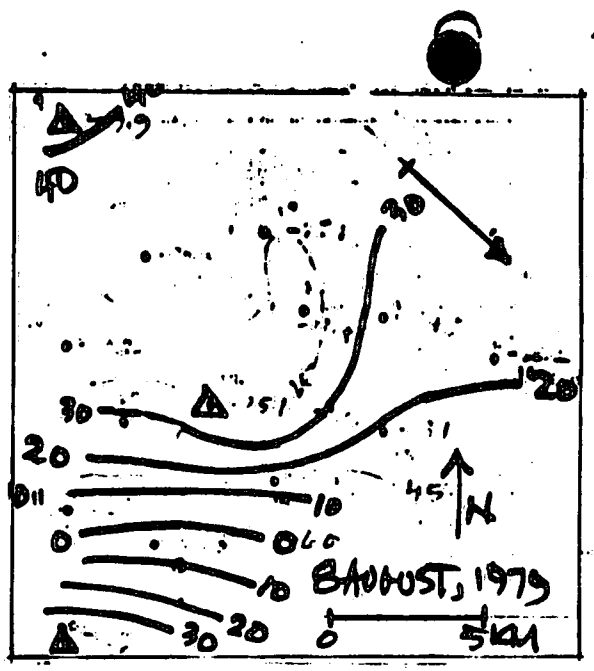
30
20
10
N
8 AUGUST, 1979
0
5KM

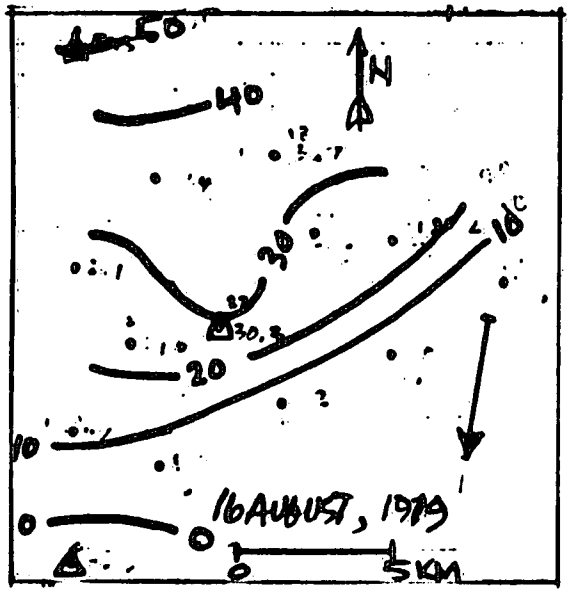
40
30
20
10
N
16 AUGUST, 1979
0
5KM

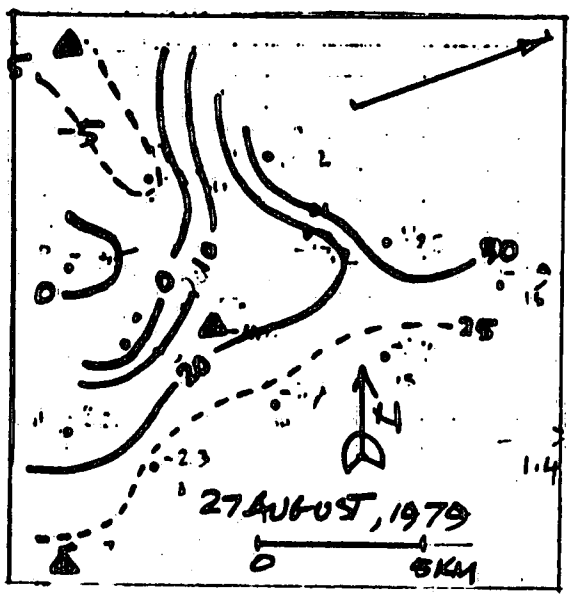
30
25
20
10
N
27 AUGUST, 1979
0
5KM

FIGURE 5